

Article

Direct Power Control Based on Modified Sliding Mode Controller for a Variable-Speed Multi-Rotor Wind Turbine System Using PWM Strategy

Habib Benbouhenni ¹, Zinelaabidine Boudjema ², Nicu Bizon ^{3,4,5,*}, Phatiphat Thounthong ^{6,7}
and Noureddine Takorabet ⁷

- ¹ Department of Electrical & Electronics Engineering, Faculty of Engineering and Architecture, Nisantasi University, 34481742 Istanbul, Turkey; habib.benbouenni@nisantasi.edu.tr
 - ² Laboratoire Génie Électrique et Energies Renouvelables (LGEER), Department of Electrical Engineering, Hassiba Benbouali University of Chlef, Chlef 02000, Algeria; z.boudjemaa@univ-chlef.dz
 - ³ Faculty of Electronics, Communication and Computers, University of Pitesti, 110040 Pitesti, Romania
 - ⁴ Doctoral School, Polytechnic University of Bucharest, 313 Splaiul Independentei, 060042 Bucharest, Romania
 - ⁵ ICSI Energy Department, National Research and Development Institute for Cryogenic and Isotopic Technologies, 240050 Ramnicu Valcea, Romania
 - ⁶ Renewable Energy Research Centre (RERC), Department of Teacher Training in Electrical Engineering, Faculty of Technical Education, King Mongkut's University of Technology North Bangkok, 1518 Pracharat 1 Road, Wongsawang, Bangsue, Bangkok 10800, Thailand; phatiphat.t@fte.kmutnb.ac.th
 - ⁷ Group of Research in Electrical Engineering of Nancy (GREEN), University of Lorraine-GREEN, F-54000 Nancy, France; noureddine.takorabet@univ-lorraine.fr
- * Correspondence: nicu.bizon@upit.ro



Citation: Benbouhenni, H.; Boudjema, Z.; Bizon, N.; Thounthong, P.; Takorabet, N. Direct Power Control Based on Modified Sliding Mode Controller for a Variable-Speed Multi-Rotor Wind Turbine System Using PWM Strategy. *Energies* **2022**, *15*, 3689. <https://doi.org/10.3390/en15103689>

Academic Editor: Abu-Siada Ahmed

Received: 5 April 2022

Accepted: 16 May 2022

Published: 18 May 2022

Publisher's Note: MDPI stays neutral with regard to jurisdictional claims in published maps and institutional affiliations.



Copyright: © 2022 by the authors. Licensee MDPI, Basel, Switzerland. This article is an open access article distributed under the terms and conditions of the Creative Commons Attribution (CC BY) license (<https://creativecommons.org/licenses/by/4.0/>).

Abstract: A robust and improved control scheme of a variable speed multi-rotor wind turbine (MRWT) system with a doubly fed asynchronous generator (DFAG) is displayed in this work. In order to improve the performances and effectiveness of the traditional direct power control (DPC) strategy of the DFAG, a new kind of sliding mode controller (SMC) called modified SMC (MSMC) is proposed. The most important advantage of the DPC-MSMC strategy is to reduce the power ripples and improve the quality of the currents provided to the grid. In addition, to control the rotor inverter, a pulse width modulation (PWM) technique is used. The proposed DPC-MSMC strategy was modeled and simulated using MATLAB/Simulink software. The simulation results showed that the ripples in stator currents, active and reactive powers and torque were considerably reduced for the proposed DPC-MSMC strategy compared to the traditional DPC. Additionally, the proposed DPC-MSMC method works excellently to reduce the total harmonic distortion (THD) of the stator current in the case of variable wind speed. On the other hand, a robustness test against parametric variations showed and confirmed the robustness of the proposed technique compared to the classical method.

Keywords: doubly fed asynchronous generator; variable-speed multi-rotor wind turbine system; direct power control; modified SMC technique; total harmonic distortion

1. Introduction

The tremendous technological developments recorded in recent years have played a major and important role in increasing wind power and making use of one of the most exploited renewable energies in the world, especially in advanced industrialized countries [1,2]. This development has been accompanied and contributed by many research teams in different countries around the world, where numerous articles have been published in important scientific journals [3–5].

Wind turbines are divided into two large families according to their speed of rotation—we distinguish wind turbines with fixed speeds and those with variable speeds. Due to

the variable nature of wind speed, those with variable speeds are the most commonly used [6,7].

After much bibliographic research, it has been found that the doubly fed asynchronous generator (DFAG) is the most used machine in wind turbine systems [8–12]. The main feature of this generator is that it can be controlled from the rotor side through a power inverter sized one-third smaller than in the case of other machines controlled by the stator [13]. Additionally, this generator is more robust and has minimal maintenance compared to other generators such as asynchronous generators.

Among the large number of control methods and techniques of electrical machines existing in the literature, that based on field orientation remains the most used and marketed due to its simplicity and efficiency. Among the most famous methods used to control the DFAG and have been widely used in renewable energies is direct torque control (DTC) [14], sliding mode control (SMC) [15], backstepping control [16], vector control [17], synergetic control [18], direct power control (DPC) [19], hybrid control [20], field-oriented control (FOC) [21], and high-order SMC strategy [22]. In Table 1, a comparison is made between the various existing methods that were applied to the DAPG-based wind turbine system, using criteria such as the degree of complexity, the ripple ratio, the dynamic response, etc. From this table, FOC strategy control is one of the ways proportional-integral (PI) controllers are efficiently used. This method is among the most famous and most widely used methods in the field of controlling electrical machines. This method can be easily accomplished. However, the use of conventional PI regulators and its large dependence on the parameters of the control system represents the main disadvantage of this method. The use of robust controllers capable of overcoming this problem has been the subject of much scientific research in recent years.

Table 1. A comparative study between the different methods used in wind turbine.

	DPC	Hybrid Control	Backstepping Control	DTC	FOC	Synergetic Control
Robustness	Robust	More robust	Robust	Robust	Not robust	Robust
Control of inverter	Switching table	PWM	PWM	Switching table	PWM	PWM
Quality of current	Acceptable	High	Good	Acceptable	Weak	Good
Experimentation	Easy	Difficult	Difficult	Easy	Difficult	Easy
Dynamic response	Fast	Fast	Fast	Fast	Slow	Fast
Simplicity	Simple	Complicated	Complicated	Simple	Rather complicated	Simple
Controller	Hysteresis comparator	Intelligent/Nonlinear controller	-	Hysteresis comparator	PI controller	Synergetic controller
THD	Medium	Low	Medium	Medium	High	High

To improve the performance and effectiveness of electrical machine control methods, artificial intelligence is used as a means to reduce road defects. In [23], neural networks were used to improve the performance and effectiveness of the DPC method for an DFAG-based wind turbine system. Through the results, the use of neural networks leads to reducing the ripples of current, active power and torque. Additionally, it improves the dynamic response to active and reactive power compared to the traditional strategy. In [24], the author introduces a fuzzy logic controller to the DTC method with the aim of improving durability and obtaining high quality current in the electrical network. The proposed strategy is more robust than traditional DTC strategy. Another intelligent method based on the genetic algorithm (GA) was used to improve the performance and effectiveness of the DPC method by using the perfect proportional and integral gains of the PI controller [25]. This proposed DPC method is simple, uncomplicated, easily accomplished, and more robust compared to the classical DPC method. DTC strategy and ant colony optimization (ACO) algorithm was combined to control the DFAG-based wind turbine system [26]. The proposed DTC strategy is more robust compared to the traditional DTC strategy with a PI controller. Additionally, the DTC based on the ACO method reduced the total harmonic distortion (THD) value by 40.08% compared to the traditional DTC-PI method. This ratio is very good, which indicates the effectiveness of the ACO method in improving performance compared to the traditional methods such as the PI controller.

Another approach to improving the performance and efficiency of methods such as DPC is based on the use of nonlinear methods. These nonlinear methods are known to be robust and not affected by changing parameters of the system under study. In [27], the DPC based on backstepping control method is used to control the DFAG-based wind turbine system. The results showed that the proposed DPC-BC technique is better in terms of reducing the value of the ripples, torque, current and active power, compared to the classical DPC method. This reduction in the ratio of ripples was very significant, which indicates the effectiveness of the combination of two different methods (DPC strategy and BC technique). Additionally, an improvement in the dynamic response compared to the traditional DPC methods is observed. Another non-linear method was used in [28] to improve the performance and efficiency of the traditional DPC method, where a second-order sliding mode controller (SOSMC) is used to control both the effective power and the reactive power. This nonlinear method is more robust than traditional SMC strategy. The proposed DPC-SOSMC strategy is robust and easy to implement. An adaptive-gain SOSMC controller has been proposed in [29].

As it is known, sliding mode control is a type of non-linear method that appeared in the early 1970s. This method was suggested by Emelyanov and Utkin in order to overcome the obstacles of using a PI controller [30–34]. The SMC theory was used in many areas such as power electronics and control. Durability is among the most famous advantages of this method compared to the classic methods. The use of the SMC controller in systems leads to improved performance and overcoming defects when the parameters of the studied system are changed. On the other hand, this technique has shown its great efficiency and robustness in the field of rotating machines control. However, despite its qualities, the presence of the undesirable chattering phenomenon has greatly reduced its use. This phenomenon, created by a discontinuous part of the control, has been the subject of hundreds of research works that have attempted to attenuate it. Several methods have been suggested to remedy this problem such as the smooth approximation of discontinuous part [35], techniques based on artificial intelligence [36–39], high order sliding mode [40].

Other attractive methods have lately been applied and have proven good results such as fractional-order SMC [41–44], adaptive terminal and variable exponential discrete-time sliding mode reaching laws [45,46], adaptive high order sliding mode [47], etc.

Further researchers have proposed hybrid solutions such as H_∞ sliding mode [48], backstepping SMC [49,50], sliding mode with passivity-based control [51,52], and predictive SMC [53,54].

So, a new nonlinear method, called modified slide mode control (MSMC), has been proposed and tested in this paper to prove its robustness and great efficiency in mitigating the chattering phenomenon in DFAG operation. This controller is first proposed and designed in this paper, being based on a change in the traditional SMC technique with the aim of obtaining a simpler method of application in systems, especially complex ones. The Lyapunov theory is employed to define the stability regions of the designed MSMC parameters. In this paper, the MSMC strategy is proposed to achieve the DPC technique of the DFAG-based multi-rotor wind turbine (MRWT) system and keep the THD value of the stator current at the minimum value. The main contribution of this paper is to provide a combination strategy of the DPC method and proposed MSMC technique to minimize the ripples for reactive power, torque, active power, and stator current of the DFAG-based MRWT system. Additionally, the proposed DPC-MSMC strategy is a robust, simple, and easy to implement algorithm. The main contributions of the proposed designed DPC strategy are as follows: (1) reduces ripples in the current, reactive, and active powers; (2) increases the robustness and stability of the controlled system; (3) provides a simple and less complex method to be used to control complex systems; (4) improves the THD value of the rotor and stator currents; (5) improves the performance and effectiveness of the traditional DPC strategy; (6) simplifies the use of the slide mode control technique.

In additions, an empirical comparison study between the traditional hysteresis comparators is achieved. Additionally, a statistical comparison was made to assess the sig-

nificance of the proposed strategy against some published control techniques in terms of underestimating the THD value of the electric current. Furthermore, the performance of the DPC-MSMC technique is compared with conventional DPC with a lookup table for reference tracking and parameter variations.

The paper is prepared as follows. The modeling of the DFAG-based variable speed MRWT system is given in Section 2. The proposed MSMC technique is dedicated in Section 3. Classical DPC strategy of the DFAG-based MRWT system is explained in Section 4. Section 5 describes the DPC strategy based on the proposed MSMC technique of the grid side converter (GSC). In Section 6, simulation results are shown and discussed. Finally, the paper's conclusions are presented in Section 7.

2. Model of DFAG-MRWT System

The electric power generation system used in this work is illustrated in Figure 1, where a multi-rotor wind turbine is used to rotate the generator (DFAG), and P_s^* and Q_s^* represent the references for active and reactive power. The latter is fed by two inverters with different working principles.

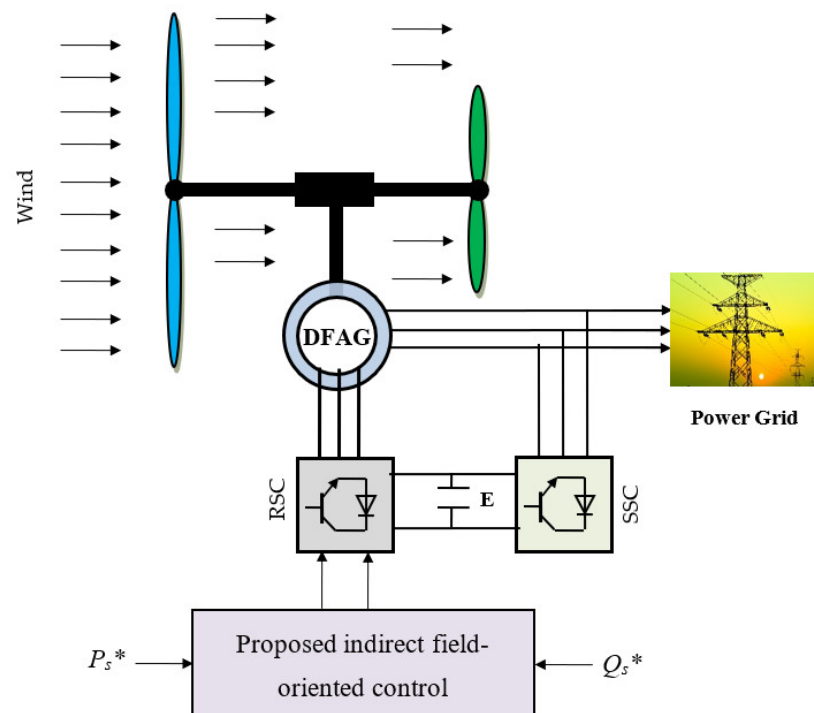


Figure 1. Structure of the MRWT system.

In this work, a MRWT system was used in order to obtain more energy from the wind, as this turbine is two turbines located in the same axis. This system has been studied in several scientific works in order to improve the performance of the classic turbine [55–57]. MRWT system is a large turbine connected to a turbine of small power and rotating in the same direction. The torque produced by the MRWT system is the product of the two torques of the large turbine and the small turbine [58]. The mechanical energy gained from wind by a multi-rotor wind turbine system is shown in Equation (1).

$$P_t = P_{ST} + P_{LT} \quad (1)$$

The torque produced by the MRWT system is the sum of the two torques of the large and small turbine, where the torque produced is used to rotate the DFAG. Equation (2) represents the torque of a multi-rotor wind turbine.

$$T_t = T_{ST} + T_{LT} \quad (2)$$

where P_t and T_t are the total power and torque of the MRWT system, T_{LT} and T_{ST} are the torque of the large and small wind turbines, and P_{LT} and P_{ST} are the mechanical power of the large and small wind turbines.

The torque produced by the small turbine and the large turbine is related to both wind speed (w_{ST} and w_{LT}), the air density (ρ), the large turbines (R_{ST} , R_{LT}), and the coefficient of power (C_p). These two torques are expressed by Equations (3) and (4) [56].

$$T_{LT} = \frac{C_p}{2\lambda_{LT}^3} \rho \cdot \pi \cdot R_{LT}^5 \cdot w_{LT}^2 \quad (3)$$

$$T_{ST} = \frac{C_p}{2\lambda_{ST}^3} \rho \cdot \pi \cdot R_{ST}^5 \cdot w_{ST}^2 \quad (4)$$

To calculate the C_p , Equation (5) is used, where this is a coefficient related to both tip speed ratio (λ) and pitch angle (β).

$$C_p(\beta, \lambda) = \frac{1}{0.08\beta + \lambda} + \frac{0.035}{\beta^3 + 1} \quad (5)$$

The mechanical power gained from the wind for each turbine is represented by Equations (6) and (7) [55].

$$P_{ST} = \frac{C_p(\beta, \lambda)}{2} \rho \cdot S_{ST} \cdot w_{ST}^3 \quad (6)$$

$$P_{LT} = \frac{C_p(\beta, \lambda)}{2} \rho \cdot S_{LT} \cdot w_{LT}^3 \quad (7)$$

The value of the tip speed ratios of the small turbine and the large turbine are given in Equations (8) and (9), respectively [58].

$$\lambda_{ST} = \frac{w_{ST} \cdot R_{ST}}{V_{ST}} \quad (8)$$

$$\lambda_{LT} = \frac{w_{LT} \cdot R_{LT}}{V_{LT}} \quad (9)$$

To calculate the wind speed at any point between the large and small turbines, Equation (10) is used. Where this speed is related to the distance between the two turbines, as well as a constant value ($C_T = 0.9$) [57].

$$V_x = V_{LT} \left(1 - \frac{1 - \sqrt{(1 - C_T)}}{2} \left(1 + \frac{2x}{\sqrt{1 + 4x^2}} \right) \right) \quad (10)$$

where V_{LT} is the wind speed of the large turbine and x is the distance between the center of the large and small turbines.

In this work, the distance between the big turbine and the small turbine is 15 m. The turbine used in this work is used to rotate an electric generator of the type DFAG in order to obtain electrical energy. This generator is used because of its durability, ease of control, low maintenance and gives excellent results in case of variable wind speed. The generator is a transformer, which converts the mechanical energy gained from the wind into electrical energy. The latter is used to feed the electrical network. So, the generator used contains two main parts, the electrical part and the mechanical part. On the other hand, the Park

transform is used to give the generator the mathematical form. Equation (11) represents the electrical part of the generator, presenting the voltage and flux of the generator.

$$\left\{ \begin{array}{l} V_{dr} = R_r I_{dr} - \omega_r \Psi_{qr} + \frac{d}{dt} \Psi_{dr} \\ V_{qr} = R_r I_{qr} + \omega_r \Psi_{dr} + \frac{d}{dt} \Psi_{qr} \\ V_{qs} = R_s I_{qs} + \omega_s \Psi_{ds} + \frac{d}{dt} \Psi_{qs} \\ V_{ds} = R_s I_{ds} - \omega_s \Psi_{qs} + \frac{d}{dt} \Psi_{ds} \\ \Psi_{dr} = L_r I_{dr} + M I_{ds} \\ \Psi_{qr} = M I_{qs} + L_r I_{qr} \\ \Psi_{qs} = M I_{qr} + L_s I_{qs} \\ \Psi_{ds} = L_s I_{ds} + M I_{dr} \end{array} \right. \quad (11)$$

As for the mechanical part, it is expressed by Equation (12) [59,60]:

$$T_e = J \frac{d\Omega}{dt} + f\Omega + T_r \quad (12)$$

Generator torque (T_e) is related to both stator flux and rotor current and can be expressed by Equation (13) [35].

$$T_e = 1.5p \frac{M}{L_s} (-\Psi_{sd} I_{rq} + \Psi_{sq} I_{rd}) \quad (13)$$

On the other hand, the active and reactive power can be calculated using Equation (14), where to calculate these two values, both stator voltage and current must be measured. In addition, the quality of the active power is related to the quality of the electric current, and to obtain a high-quality electric current, a control method must be chosen that gives excellent results in terms of current ripples and THD value.

$$\left\{ \begin{array}{l} P_s = 1.5(V_{qs} I_{qs} + I_{ds} V_{ds}) \\ Q_s = 1.5(-I_{qs} V_{ds} + V_{qs} I_{ds}) \end{array} \right. \quad (14)$$

3. Proposed Modified SMC Technique

In this part, a new idea is presented to SMC technique to improve the performance of the classical DPC method and enhance the quality of electric power generated by the DFAG integrated in the MRWT system. As it is known, SMC technique is a type of nonlinear method most widely used, as this method appeared in the late last century to overcome the problem of classical methods such as field-oriented control [61]. Among the advantages of this method is that it is robust control and can be easily accomplished [62]. In addition, the strengths of SMC lie in its parametric mismatch, external unknown disturbances, robust nature performance against uncertainties, fast convergence, and fault conditions.

Equation (15) expresses the principle of the SMC method, where there are two parts in this method are continuous control (u_{eq}) and discontinuous control (u_n) [63]. To use the SMC control method, the mathematical form of the studied system must be known, which makes this method difficult to use in the case of complex systems [64]. In addition, the problem of chatter is among the downsides of this method. This problem creates several defects in the systems such as ripples and turbulence in operation.

$$u = u_n + u_{eq} \quad (15)$$

where u_{eq} is named the equivalent control which has as an objective the compensation of the undesirable dynamics; it is used when the system enters the sliding mode. The command u_n is determined in order to verify the convergence condition despite the inaccuracy on

the model parameters [62]. Equation (16) represents the discontinuous control of the SMC technique, where K is the gain by which the SMC response is adjusted.

$$u_n = K \times \text{Sign}(e) \quad (16)$$

where e is the error or sliding surface ($e = X^* - X$) and K is the positive gain.

In the SMC method, the continuous control is calculated using the mathematical form of the studied system, which makes this method difficult to perform especially in the case of complex systems such as seven-phase induction motor [61]. In addition, the dynamic response of the classical method is somewhat heavy compared to other nonlinear methods such as the super twisting algorithm. Additionally, the use of the classical SMC method in automated systems increases energy consumption and this is not desirable.

In order to overcome the defects of the SMC method, a new idea is proposed by changing the original principle of the SMC technique, whereby the continuous control part is removed and replaced with $K_2 \times e(t)$. The proposed SMC method or modified SMC (MSMC) technique is shown in Equation (17), where both K_1 and K_2 are used to adjust the response of the proposed MSMC technique.

$$w = K_1 \times \text{Sign}(e(t)) + K_2 \times e(t) \quad (17)$$

where K_1 and K_2 are the positive constants. These gains are used to adjust and improve the response of the proposed MSMC technique.

The amplitude K_1 is chosen to be large enough to compensate for the difference in dynamics between the actual system and the reference system (given by the sliding surface) and to compensate for the co-incident disturbances.

The objective of the control law is to constrain the state trajectories of a system to reach and then stay on the sliding surface despite the presence of uncertainties on the system. In other words, the control law must make the surface of locally attractive sliding (i.e., in the vicinity of the sliding surface, all the trajectories of the system must be directed towards it). Thus, the control law must be calculated by verifying a condition ensuring the stability of the sliding surface, $S(x, t) = 0$. Such a condition is called the attractiveness condition. On the other hand, the proposed MSMC technique is more simple, more robust (being not related to the system parameters), and easy to implement compared to the traditional SMC strategy. Additionally, the proposed MSMC technique can be used in a complex system, easily replacing the classic SMC strategy. However, the use of the proposed MSMC technique makes the system fast in terms of dynamic response due to the absence of complex calculations such as derivation or integration.

The direct method of Lyapunov makes it possible to pronounce as to the stability of a state equilibrium without resorting to solving the equation of state of the system. Supposing that the equilibrium state is 0, to ensure the stability of the proposed MSMC technique, Equation (18) is used. The proposed MSMC method is a simple one, not related to the mathematical form of the studied system, and it can be accomplished easily. Moreover, the proposed MSMC method is more robust because it is not related to the parameters of the studied system, which makes it overcome the shortcomings of the classical SMC method.

$$S \times \dot{S} < 0 \quad (18)$$

The sign of a function $V(x)$, ($V(0) = 0$, $V(\infty) = \infty$), called Lyapunov's function, and that of its time derivative $\dot{V}(x) = \frac{dV(x)}{dt}$ give information on the stability of the system. $V(x)$ plays the role of an "energy" function active for the considered system. If $V(x) > 0$, $\forall x \neq 0$ and $\dot{V}(x) < 0$, the system is asymptotically stable. A class of classical Lyapunov functions for determining the condition of attractiveness is that of quadratic functions of the type.

$$V(x) = \frac{1}{2} \times S^2 \quad (19)$$

This function is positively defined in an obvious way. A necessary and sufficient condition for the slip variable $S(x, t)$ to tend to zero is that the derivative of V be defined negative.

$$\dot{V} = S \times \dot{S} < 0 \quad (20)$$

This inequality is called the attractiveness condition which is not sufficient to ensure finite time convergence to the surface. To ensure convergence of $S(x, t)$ towards 0 in finite time, a stronger condition must be respected. In the case of modes classical sliding conditions, the condition of non-linear attractiveness called η -attractive condition is generally used.

$$S \times \dot{S} \leq -\eta \times |S|, \eta > 0 \quad (21)$$

where η is a positive gain (for example, $\eta = K_1$).

It comes back, for $S \neq 0$, to

$$\dot{S} \leq -\eta \times \text{Sign}(e), \eta > 0 \quad (22)$$

We see immediately why this criterion guarantees convergence in finite time. By integration, if $S(0) > 0$, $S(t) \leq S(0) - \eta \times t$, and if $S(0) < 0$, $S(t) \geq S(0) + \eta \times t$. So, in all cases, $S(x, t)$ reaches 0 in less than $\frac{|S(0)|}{\eta}$.

Therefore, this criterion is always satisfied if the command is of the type

$$w = K_1 \times \text{Sign}(e) \quad (23)$$

To simplify the idea of the proposed MSMC method, Figure 2 is given to facilitate and clarify the concept further.

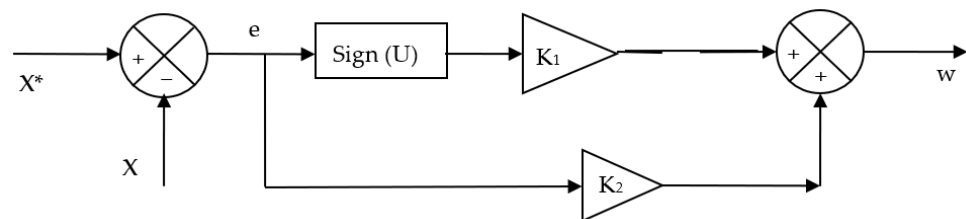


Figure 2. Schematic diagram of the proposed MSMC technique.

In the proposed MSMC technique, the $K_2 \times e(t)$ part is used in the proposed method to simplify the method and make it more suitable, especially with complex systems such as a seven-phase asynchronous motor. Additionally, it simplifies the calculations and does not complicate the use of sliding control. Moreover, it made the dynamic response more rapid compared to the classic method. The $K_2 \times Se(t)$ and $K_2 \times (de(t)/dt)$ can be used in place of $K_2 \times e(t)$, in which case these methods are called integral modified sliding mode control (IMSMC) and derivative modified sliding mode control (DMSMC), respectively. These can be the subject of further research.

This method (MSMC) is used to improve the performance of the traditional DPC method with a switching table (as explained in the next section) and the designed DPC-MSMC method is presented in Section 5 of the paper.

4. DPC Strategy

The classical DPC method is among the methods used in the field of wind energy and this is because of its simplicity and ease of implementation compared to the field-oriented control method, where in this method the active and reactive power are directly controlled by using a switching table and two hysteresis comparators [65]. This method is very similar to the direct torque control method, and the difference lies in the controlled amounts. In the direct torque control method, the torque and flux are controlled. As for the classical

DPC technique, the active and reactive power are controlled using the active and reactive power as references [66]. Figure 3 represents the principle of the classical DPC technique of DFAG placed in a MRWT system.

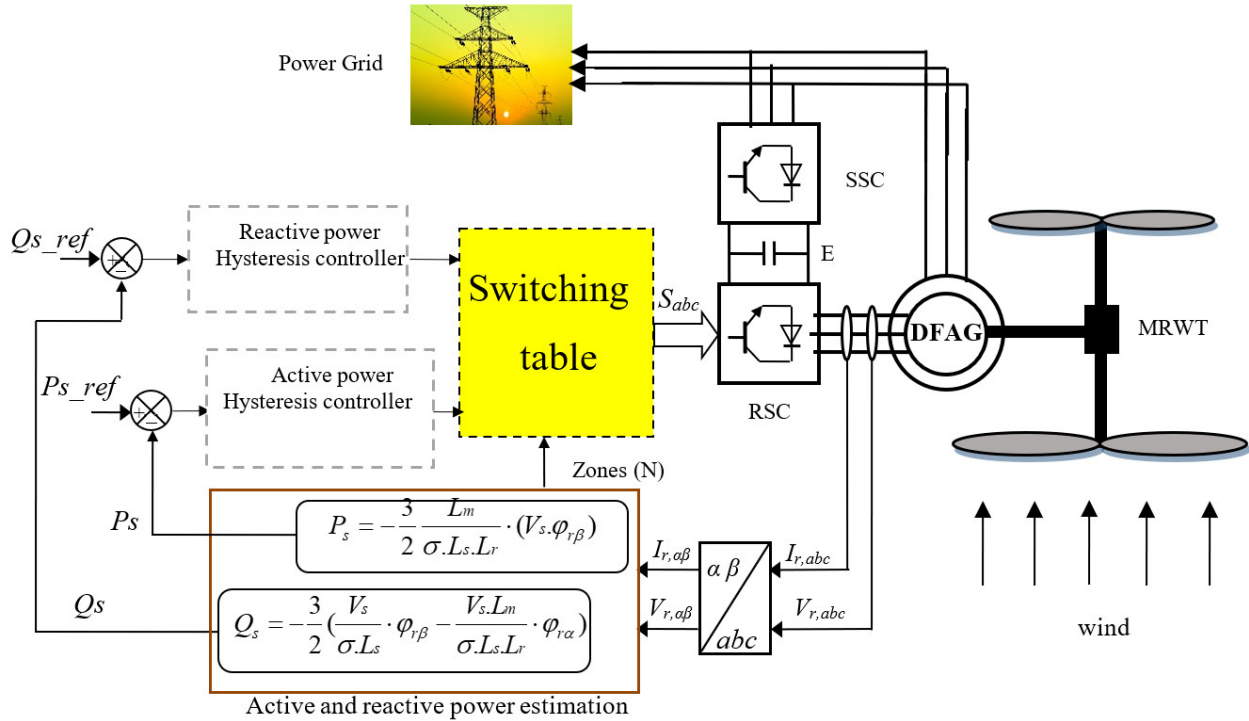


Figure 3. Classical DPC of the DFAG-MRWT system.

From Figure 3, the classic DPC method is simple and easy to perform compared to the FOC method. Moreover, the traditional DPC method gives a fast dynamic response compared to some methods such as vector control [67]. In this method, we need to estimate both the reactive power and the active power, where both current and voltage are measured in order to estimate these two values [68]. In this method, it is not necessary to know the speed of the rotor [67]. On the other hand, flux is needed to estimate the active and reactive power. Equation (24) represents both the quadrature and direct rotor flux of the generator.

$$\begin{cases} \varphi_{r\alpha} = \int_0^t (V_r - R_r i_{r\alpha}) dt \\ \varphi_{r\beta} = \int_0^t (V_r - R_r i_{r\beta}) dt \end{cases} \quad (24)$$

On the other hand, the rotor flux is given by Equation (25) [66]:

$$|\varphi_r| = \varphi_r = \sqrt{(\varphi_{r\beta}^2 + \varphi_{r\alpha}^2)} \quad (25)$$

The angle θ_r between the frame (r) and the vector φ_r , is equal to:

$$|\theta_r| = \arctg \left(\frac{\varphi_{r\beta}}{\varphi_{r\alpha}} \right) \quad (26)$$

where θ_r is the angle of the rotor flux.

Equation (27) is used to calculate the direct and quadrature stator flux. The stator flux is given by Equation (28). On the other hand, the angle of the stator flux is given

by Equation (29). This angle is of great importance in knowing the areas of reference stator voltage.

$$\begin{cases} \varphi_{s\alpha} = \int_0^t (V_s - R_s i_{s\alpha}) dt \\ \varphi_{s\beta} = \int_0^t (V_s - R_s i_{s\beta}) dt \end{cases} \tag{27}$$

$$|\varphi_s| = \varphi_s = \sqrt{(\varphi_{s\beta}^2 + \varphi_{s\alpha}^2)} \tag{28}$$

$$|\theta_s| = \arctg\left(\frac{\varphi_{s\beta}}{\varphi_{s\alpha}}\right) \tag{29}$$

where θ_s is the angle of the stator flux.

There is a relationship between tension and flux, where this relationship is shown in Equation (30). To calculate the stator and rotor flux, Equations (24) and (27) are used.

$$V_s = \varphi_s \times \omega_s \tag{30}$$

In order to estimate both the active power and the reactive power, Equation (24) through (30) are used. Equations (31) and (32) can be used to estimate the active and reactive power, respectively [57].

$$P_s = 1.5 \left(-\frac{V_s L_m}{\sigma L_s L_r} \varphi_{r\beta} \right) \tag{31}$$

$$Q_s = -1.5 \left(\frac{V_s}{\sigma L_s} \varphi_{r\beta} - \frac{V_s L_m}{\sigma L_s L_r} \varphi_{r\alpha} \right) \tag{32}$$

In the classical DPC strategy, the switching table is the main part and is the heart of the classical DPC method. This table is used to control the inverter on the generator side. Table 2 represents the switching table for the classical DPC method [65]. From this table, the control signals for the inverter gears are obtained.

Table 2. Switching table for classical DPC technique.

N		1	2	3	4	5	6
Hq	Hp						
1	1	2	3	4	5	6	1
	0	1	2	3	4	5	6
	-1	6	1	2	3	4	5
0	1	3	4	5	6	1	2
	0	4	5	6	1	2	3
	-1	5	6	1	2	3	4

As mentioned earlier, in the classical DPC method we need two hysteresis comparators in order to control the active and reactive power of the DFAG-based MRWT system. In this method, a three-level hysteresis comparator is used to control the active power, while for the reactive power, a two-level hysteresis comparator is used. Figure 4 shows the hysteresis comparators used in this method.

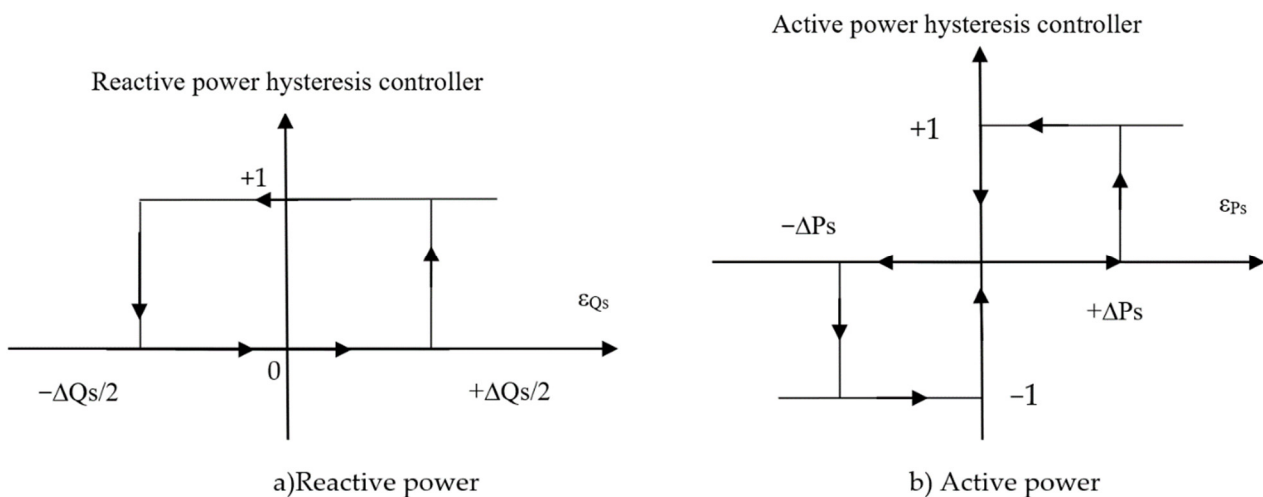


Figure 4. Scheme block of the hysteresis comparators.

The use of classical hysteresis controllers in the DPC method creates several disadvantages, including fluctuations in the level of active power, torque, reactive power, and current [69]. Additionally, this method increases the THD value of the stator current, which makes the current of an undesirable quality. In addition, we get a signal with unstable voltage at the output of the inverter, which may cause disturbances at the machine level. All of these factors lead to system-wide failures and thus increase the cost of maintenance, and this is undesirable. To overcome these difficulties, reduce maintenance costs, and improve current quality, MSMC controller is used to improve the performance of the classical DPC technique. This proposed DPC technique with the modified SMC controller is described in the next section.

5. Proposed DPC Technique

All the designed techniques for controlling the DFAG-based MRWT system do not completely eliminate the active and reactive power fluctuations. Therefore, a robust control approach must be used to ensure performance. The DFAG-based MRWT system and the MSMC-based approach is the most suitable candidate due to its simplicity and ease of application.

To improve the quality of current and active power generated by the DFAG and to reduce the ripples of torque, reactive power, flux, and current, the proposed DPC method based on a modified SMC controller (DPC-MSMC) is used. Figure 5 represents the proposed DPC-MSMC method for controlling DFAG placed in the MRWT system. The proposed DPC method based on the MSMC controller is an evolution of the classical DPC technique, in which the switching table is replaced by the PWM technique, and the hysteresis controller is replaced by the proposed MSMC controller. The designed DPC-MSMC strategy is characterized by simplicity, ease of implementation and durability compared to the classical DPC method. Additionally, the proposed strategy reduces the active power, current, and reactive power ripples compared to the FOC and DPC strategy. Therefore, the proposed strategy improves the responses dynamic of the reactive and active power of the DFAG.

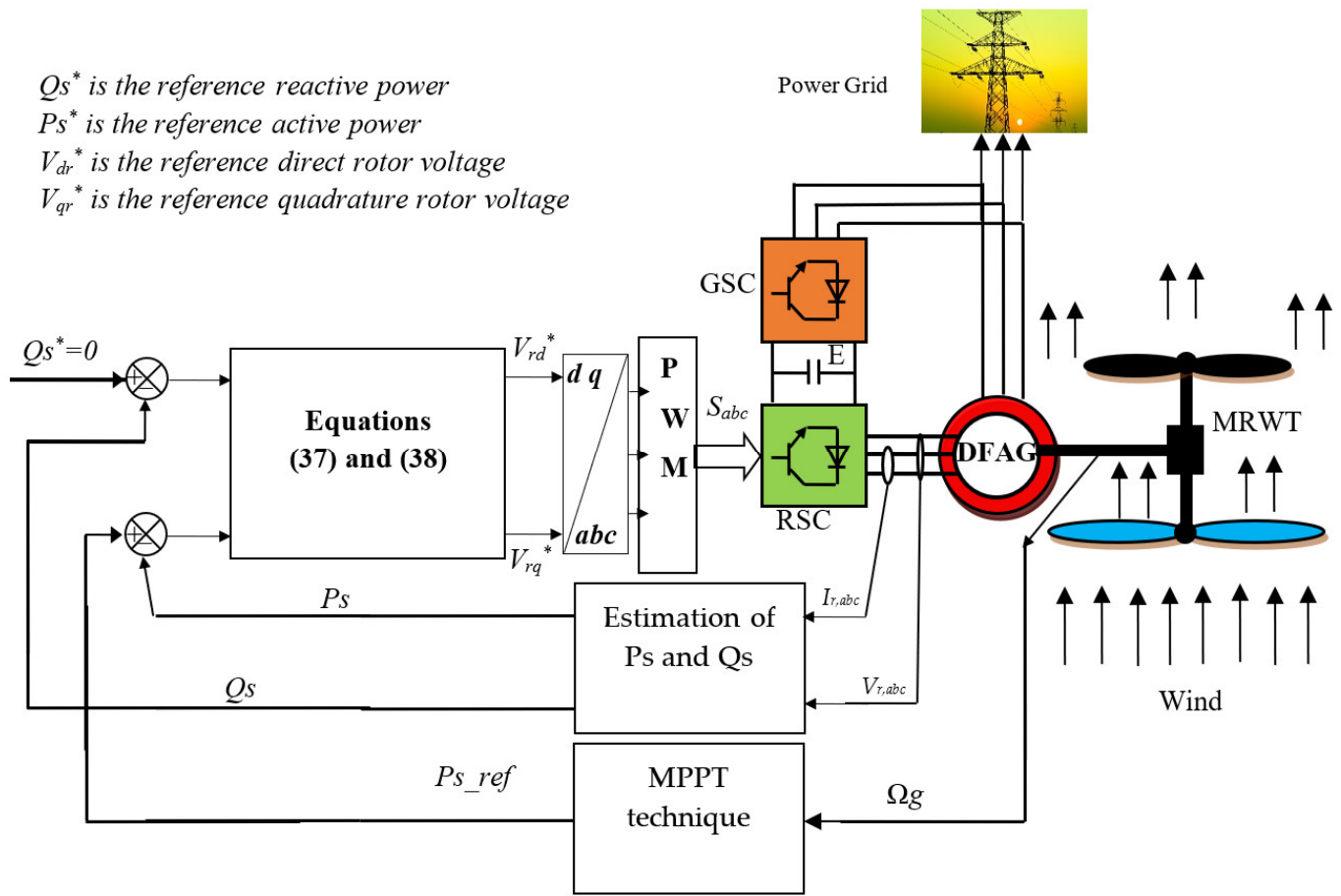


Figure 5. Proposed DPC-MSMC strategy of the DFAG-MWRT system.

In the DPC-MSMC of the DFAG system, the stator power components are controlled by regulating parts of the converter voltage at rotor side converter (RSC) circuit. Therefore, the rotor converter voltages are selected to be the control output variables.

In DPC-MSMC technique, the maximum point power tracking (MPPT) technique is used in order to get the reference value of the active power, and for the reference of the reactive power it is set to 0 Var. Moreover, Equations (31) and (32) are used to estimate both the active power and reactive power, respectively.

Control tasks for DPC strategy are to track the new reactive power, Q_s , and active power, P_s . The tracking errors are as follows:

$$\begin{cases} e_a = P_{sref} - P_s \\ e_r = Q_{sref} - Q_s \end{cases} \quad (33)$$

Equation (33) after derivation becomes as follows:

$$\begin{cases} \dot{e}_a = \dot{P}_{sref} - \dot{P}_s \\ \dot{e}_r = \dot{Q}_{sref} - \dot{Q}_s \end{cases} \quad (34)$$

The reference value for both direct and quadrature rotor voltages (V_{dr}^* and V_{qr}^*) using the proposed DPC-MSMC technique is represented by Equations (35) and (36):

$$V_{dr}^* = K_1 \times \text{Sign}(e_r) + K_2 \times e_r \quad (35)$$

$$V_{qr}^* = K_1 \times \text{Sign}(e_a) + K_2 \times e_a \quad (36)$$

where e_a and e_r are the active and reactive power errors, and K_1 and K_2 are positive gains.

From Equations (35) and (36), it can be deduced that the control laws applied to the rotor voltage dynamics are given by:

$$V_{dr}^* = K_1 \times \text{Sign} \left(Q_{sref} - Q_s \right) - \frac{3K_2}{2} \times \left(\frac{V_s}{\sigma L_s} \varphi_{r\beta} - \frac{V_s L_m}{\sigma L_s L_r} \varphi_{r\alpha} \right) \quad (37)$$

$$V_{qr}^* = K_1 \times \text{Sign} \left(P_{sref} - P_s \right) - \frac{3K_2}{2} \times \frac{V_s L_m}{\sigma L_s L_r} \varphi_{r\beta} \quad (38)$$

The modified SMC technique is proposed to generate the direct and quadrature rotor voltage references from the reactive and active power errors. Two proposed MSMC controllers are selected for reactive and active power control. The designed MSMC reactive and active power controllers of the DFAG-based MRWT system is shown in Figure 6. This proposed MSMC controller is more simple, more robust, and easy to implement. Additionally, this proposed method is not related to the parameters of the studied system, which makes it more robust and has fewer ripples compared to the classical DPC method. In Table 3, a comparative study is given between the classical DPC method and the proposed DPC-MSMC strategy. From this table, the proposed DPC-MSMC technique is much better than the classical DPC method in all aspects. Among the advantages of using the proposed MSMC controller is the mitigation of the effect of chattering resulting in an upgrade in operational performance due to the exclusion of the chattering part in the classical method. Moreover, the use of the proposed control unit significantly improves torque and reactive power compared to the traditional method. The proposed controller reduces the ripples, the active and the reactive powers, and increases the stabilization ratio.

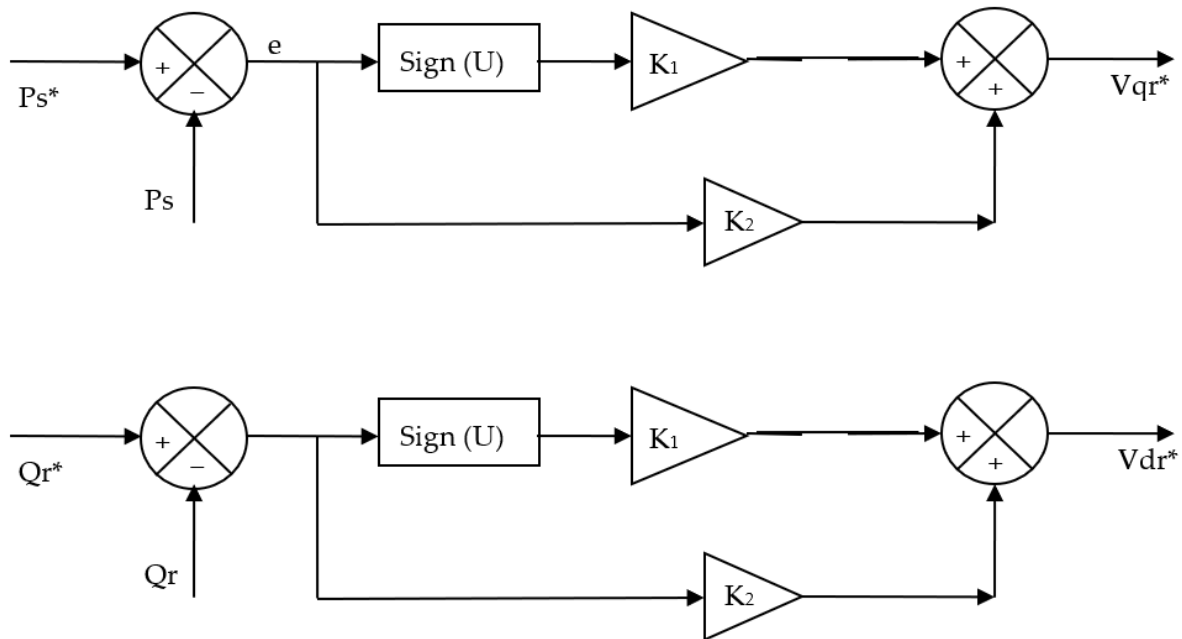


Figure 6. Block diagram of the MSMC active and reactive power controllers.

Table 3. Comparative study between the classical DPC strategy and the designed DPC-MSMC technique.

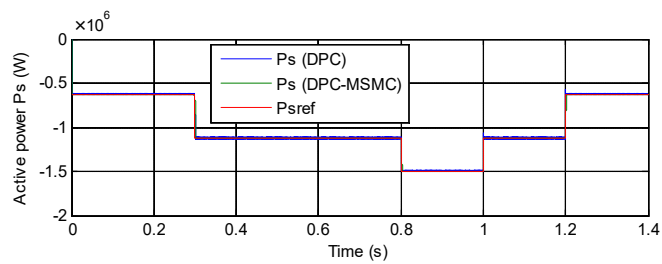
	Designed DPC-MSMC	DPC Technique
Block of estimation	Yes	Yes
Hysteresis comparator	No	Yes
Switching table	No	Yes
Robustness	High	Low
THD value of current	Low	High
Dynamic response	Fast	Slow
Power ripple	Low	High
Implementation	Easy	Easy
Simplicity	Simple	Simple
Applied to multi-phase generator	Easily	Complicated
Completion cost	Not expensive	Not expensive
Controller used	MSMC controller	Hysteresis comparator
Steady-state error	High	Low
Current quality	High	Low
Power quality	High	Low

6. Results

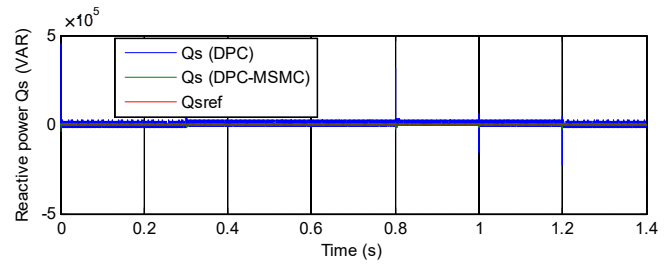
Control by DPC-MSMC technique, with the choice of stator active and reactive powers as well as sliding surfaces, was validated by numerical simulation using Matlab/Simulink software. The proposed DPC-MSMC technique is compared with the classical DPC strategy in terms of ripples of active power, torque, current, reactive power and THD value of electric current. In this work, three tests were proposed to verify the robustness of the proposed DPC-MSMC technique, where the tests are a test in the case of variable wind speed, robustness test, and a steps speed wind turbine test. The DFAG used is the same as that used in [70,71].

A. Steps speed wind test

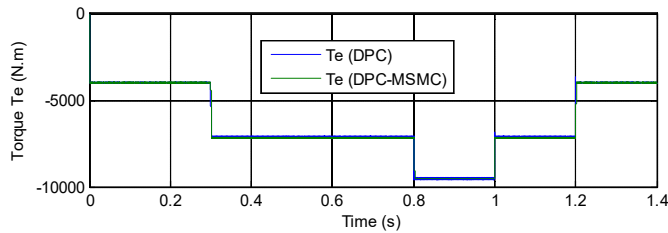
In this test, the wind speed has the form of steps, where the results obtained from this test are represented in Figure 7. From this figure, it can be seen that the active power and the reactive power follow well the references with preference over the proposed DPC-MSMC technique in terms of dynamic response (see Figure 7a,b). It is noted that a negative sign “–” implies on active power generation absorption by DFAG. The torque and current of the generator are represented in Figure 7c,d, respectively. From the two figures, it can be seen that the torque and the current take the same form as the active power and their value is related to the wind speed. In addition, the increase in wind speed leads to an increase in the value of both torque and current. Regarding the response time for the reactive power, it was 1 millisecond for the classical DPC method and 0.02 milliseconds for the designed DPC-MSMC strategy, where the designed strategy reduced the response time by 98% compared to the traditional DPC technique. Additionally, the designed DPC-MSMC strategy gave a fast response time for both torque and active power compared to the classical DPC technique. The THD value of the electric current is represented in Figure 7e,f for both the classical and the proposed DPC-MSMC technique, respectively. It is worth mentioning that the proposed DPC-MSMC technique gave a lower THD value than the classical method, and the THD reduction ratio is about 76.82%. On the other hand, the proposed DPC-MSMC technique minimized the undulations in the reactive power, current, active power, and torque compared to the traditional DPC strategy. Figure 8 presents the zoom in the reactive power, torque, and active power. The value of the ripples of reactive power, torque, active power and current are shown in Table 4. Through this table, the proposed DPC-MSMC technique reduced the ripples of current, reactive power, torque, and active power compared to the classic DPC strategy by a ratio of 75%, 92.64%, 75%, and 80%, respectively.



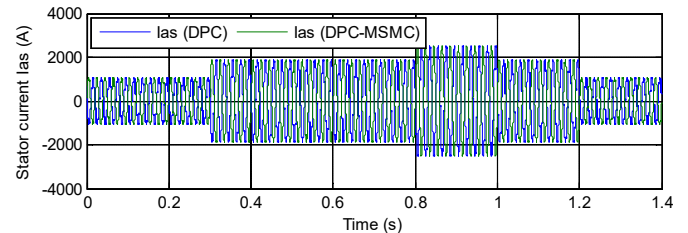
(a) Active power



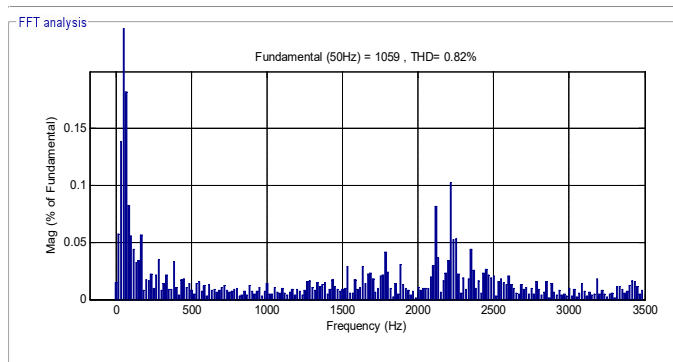
(b) Reactive power



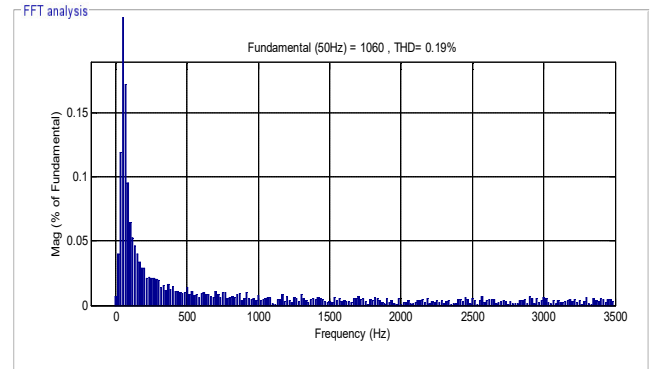
(c) Torque



(d) Stator current

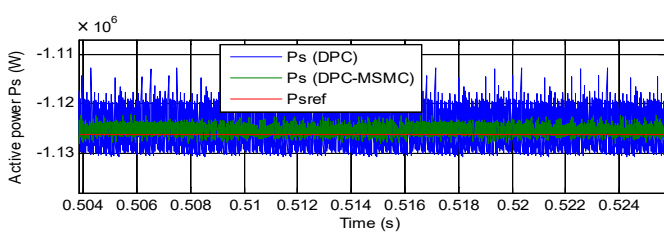


(e) THD value of stator current (DPC)

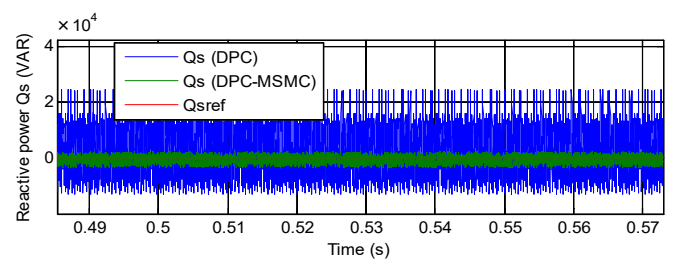


(f) THD value of stator current (DPC-MSMC)

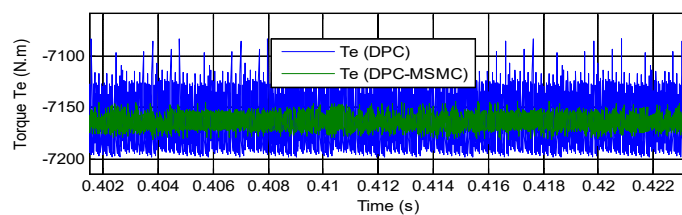
Figure 7. Simulated results from the steps speed wind test.



(a) Active power



(b) Reactive power



(c) Torque

Figure 8. Zoom in the reactive power, torque, and active power (steps speed wind test).

Table 4. Comparison of ripple values between the proposed and the classical DPC method (steps speed wind test).

	Reactive Power (VAR)	Torque (N·m)	Active Power (W)	Stator Current (A)
DPC	34,000	100	15,000	20
DPC-MSMC	2500	25	3000	5
Ratios	92.64%	75%	80%	75%

At the time moment of 1.101 s, the steady-state error for the active power was 4000 W for the classic DPC technique and 1300 W for the designed DPC-MSMC strategy. With these values, the designed strategy reduced steady-state error about 67.5% compared to the classical DPC method. As for the reactive power, the steady-state error was 5000 VAR and 2800 VAR for both the classical and the designed strategy, respectively. So, the designed DPC-MSMC strategy reduced steady-state error by 44% compared to the traditional DPC technique.

B. Variable-speed test

A variable wind speed is used in this test in order to know the change in the behavior of the proposed DPC-MSMC technique compared to the classical DPC strategy, where the results are shown in Figure 9. Through this figure, the active and reactive power follow the references well for the two methods (see Figure 9a,b) with many ripples for the classical technique compared to the proposed DPC-MSMC technique (see Figure 10a,b). Additionally, the current and the torque have the same shape as the active power (see Figure 9c,d), and the higher the active power, the higher the value of both torque and current and vice versa.

The proposed DPC-MSMC technique has reduced torque ripples compared to the classical DPC method (see Figure 10c). Moreover, the proposed DPC-MSMC technique provided the best value for THD compared to the classical DPC strategy (see Figure 9e,f) and the reduction ratio was about 71.63%. The ripples of torque, active power, reactive power and current are recorded in Table 5. Through this table, the proposed DPC-MSMC technique reduced ripples by 55%, 74.42%, 67%, and 91.33% for current, active power, torque, and reactive power, respectively, compared to the classical DPC method. On the other hand, the designed DPC-MSMC improved the dynamic response of both active and reactive power of the DFAG compared to the conventional DPC technique. At 0.9585 s, the steady state error for active power is approximately 4900 W and 50 W for traditional and designed control technique, respectively. Additionally, the steady state error of the reactive power was 5000 VAR and 1000 VAR for the traditional and proposed strategy, respectively. Consequently, the designed technique reduced the steady-state error rate by approximately 98.98% and 80% for active and reactive power, respectively, compared to the conventional DPC strategy. These results show the effectiveness of the designed DPC-MSMC technique in improving the performance and features of the classical DPC method. In the next test, the generator parameters are changed in order to study the behavior of the proposed DPC-MSMC technique in the event of a problem.

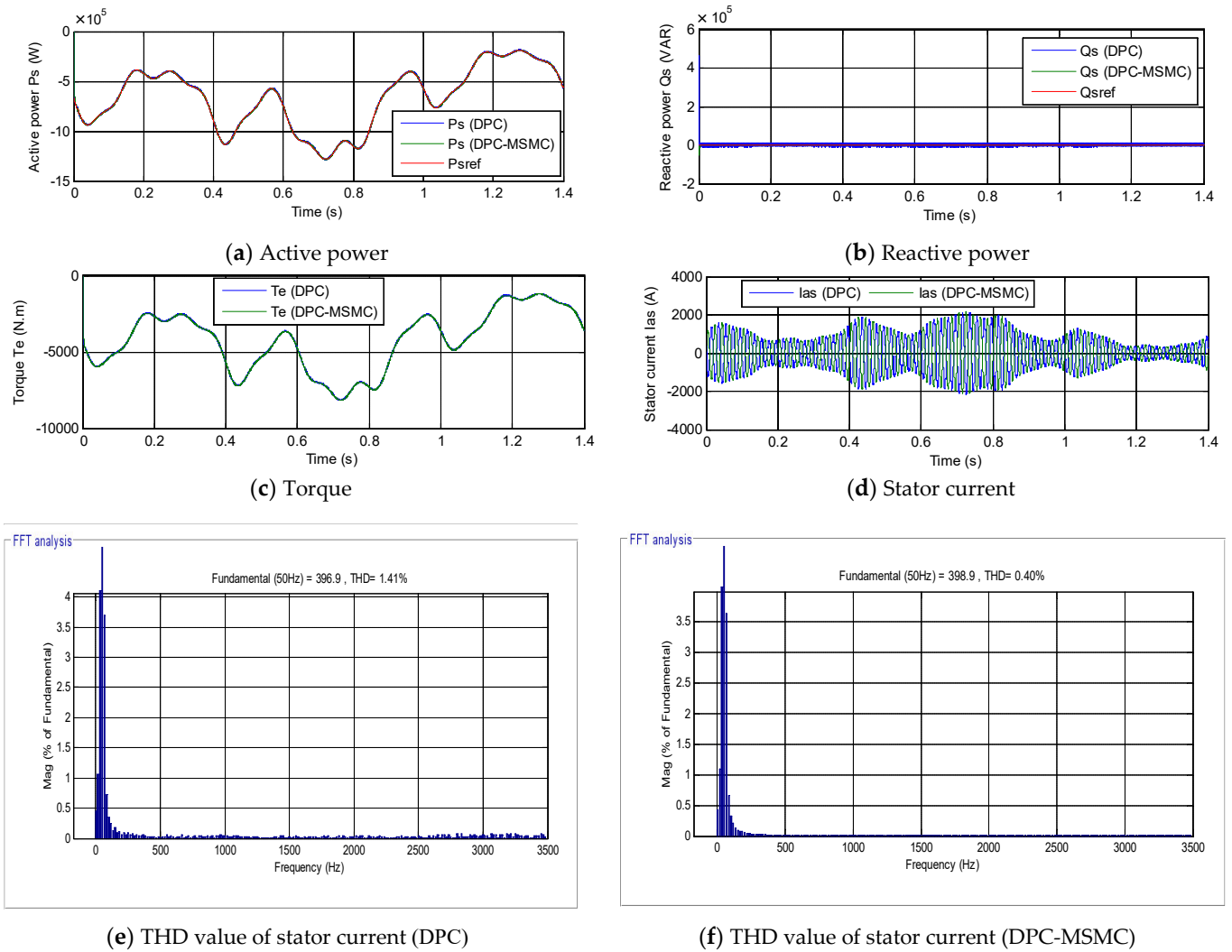


Figure 9. Simulated results from the variable-speed test.

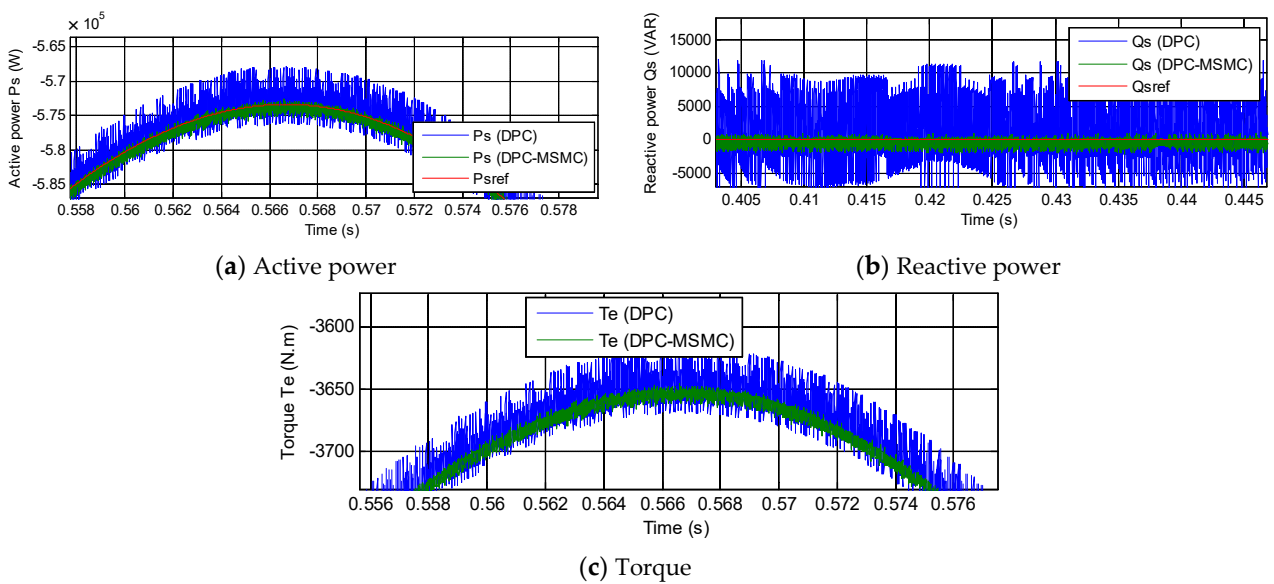


Figure 10. Zoom in the reactive power, torque, active power and current (variable-speed wind test).

Table 5. Comparison of ripple values between the designed and the traditional DPC technique (variable speed wind test).

	Reactive Power (VAR)	Torque (N·m)	Current (A)	Active Power (W)
DPC	15,000	50	20	7000
DPC-MSMC	1300	16.50	9	1790
Ratios	91.33%	67%	55%	74.42%

C. Robustness test

In this test, the behavior of the proposed DPC-MSMC technique is studied in comparison with the classical DPC strategy in case of changing L_s , L_r , R_s , L_m , and R_r to the following new values 0.00685 H, 0.0068 H, 0.024 Ω , 0.00675 H, and 0.042 Ω , respectively. The obtained results are shown in Figure 11. In this test, the classical DPC strategy is affected more by changing the machine parameters compared to the DPC-MSMC technique, and this effect is observed through the ripples of torque, reactive power, current and active power (see Figure 12a–c). Moreover, the reactive power and the active power follow the references well, despite the modification of the generator parameters (see Figure 11a,b). Additionally, the designed DPC-MSMC strategy improved the dynamic response of both reactive and active power of the DFAG-based MRWT system compared to the traditional DPC strategy.

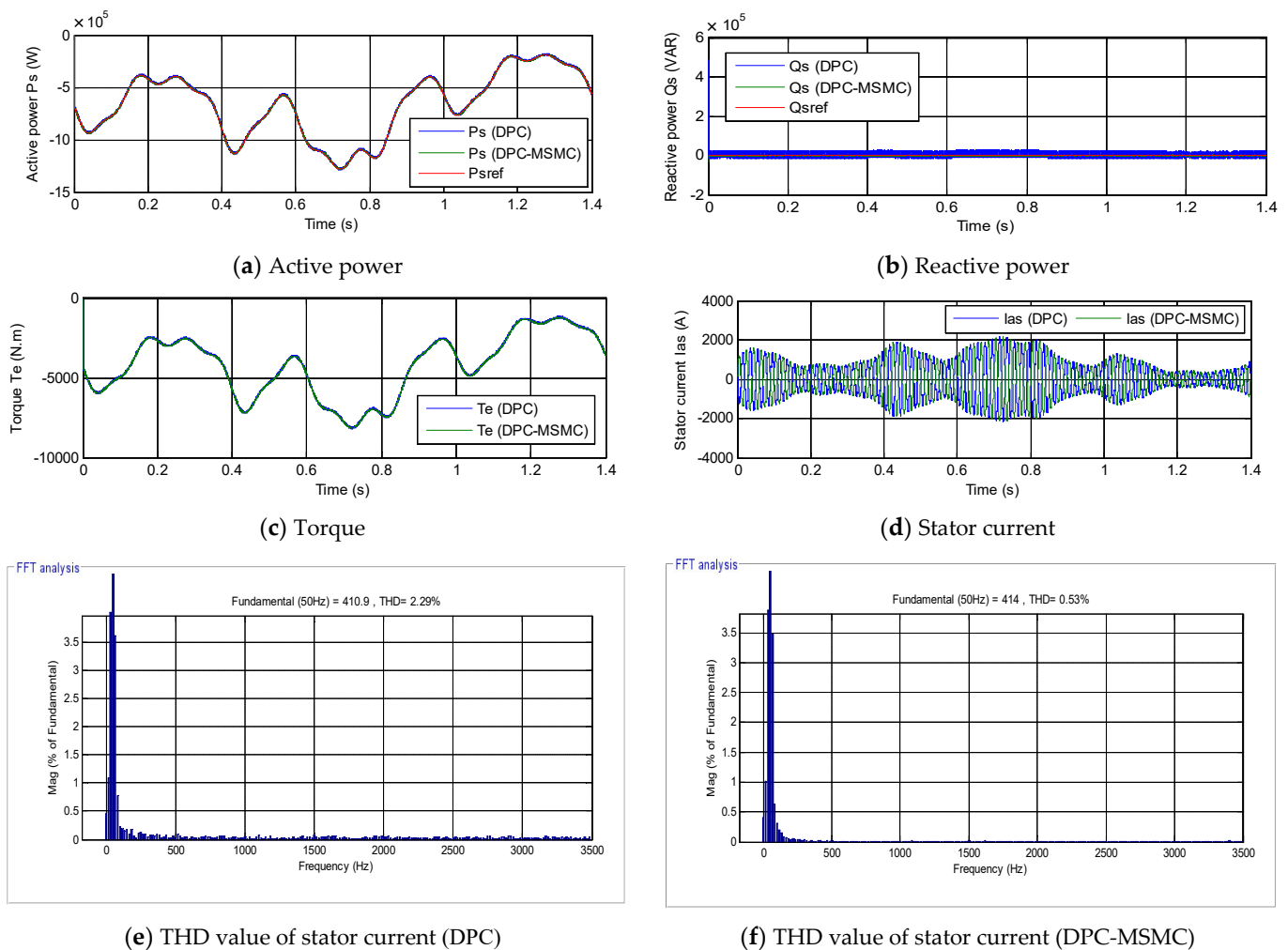


Figure 11. Simulated results from the robustness test.

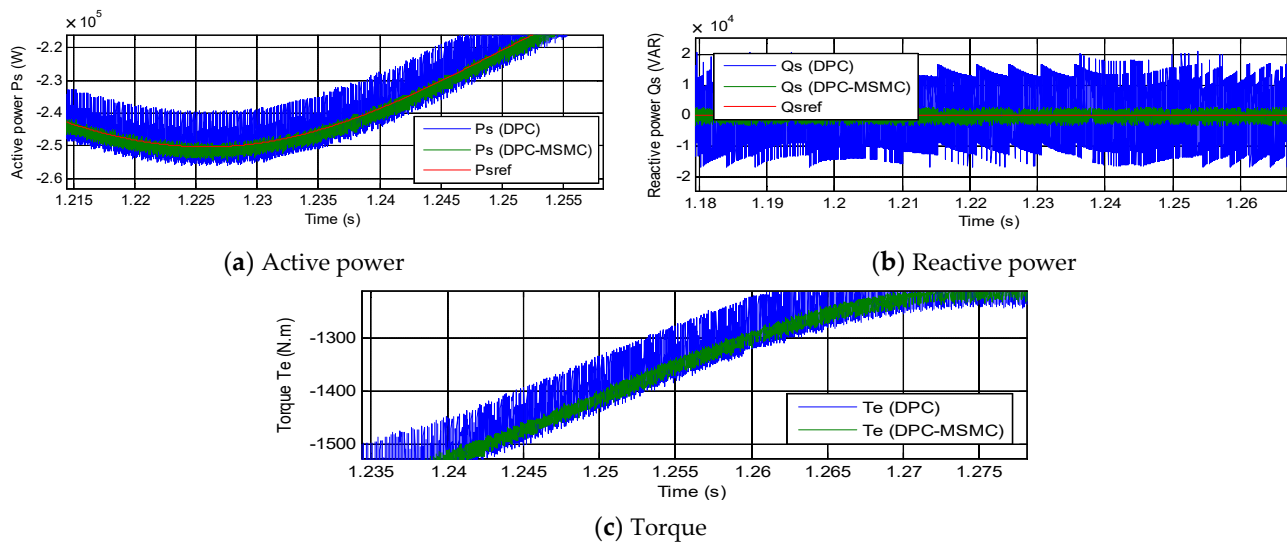


Figure 12. Zoom in the reactive power, torque, active power and current (robustness test).

The current and torque take the same form as the active power, and their value remains related to the wind speed and the studied system (see Figure 11c,d). The steady state error in this test was calculated at 0.2 s, being 7740 W and 2260 W for the conventional strategy, respectively, proposed. Consequently, the proposed DPC-MSMC strategy reduced the steady-state error value of the active power by 70.80%, compared to the conventional DPC strategy. In the case of reactive power, the value of steady-state error in this test was also calculated at the moment of 0.2 s. The steady-state error values were 18,400 VAR and 2400 VAR for for the traditional and proposed strategy, respectively. Accordingly, the designed DPC-MSMC technique minimized the steady-state error value of the active power by 86.95%, compared to the conventional DPC strategy.

The THD value of the electric current for the classical and proposed DPC-MSMC technique is shown in Figure 11e,f, respectively. The proposed DPC-MSMC technique reduced the THD value by about 76.85% compared with the classical DPC strategy. On the other hand, the value of the ripples of torque, active power, current and reactive power for the classical and proposed DPC-MSMC technique are shown in Table 6. The proposed DPC-MSMC technique reduced the ripples of torque, active power, current, and reactive power by 77%, 73.33%, 76%, and 93.71% ratios, respectively. These results show the effectiveness of the proposed DPC-MSMC technique in improving the quality of current and active power.

Table 6. Comparison of ripple values between the designed and the conventional DPC strategy (robustness test).

	Reactive Power (VAR)	Torque (N.m)	Current (A)	Active Power (W)
DPC	35,000	100	30	15,000
DPC-MSMC	2200	23	7.2	4000
Ratios	93.71%	77%	76%	73.33%

The proposed DPC-MSMC technique gave a lower value for the THD of the electric current compared to several published methods as shown in Table 7, where this table represents a comparative study between the proposed DPC-MSMC technique and several published methods in terms of the THD value of the electric current.

Table 7. A comparative study between the DPC-MSMC technique and other works in terms of the value of THD.

	Techniques	THD (%)	
Ref. [71]	Genetic Algorithm-Least Squares Wavelet Support Vector Machines (GA-LS-WSVM) method	3.39	
Ref. [72]	Field-oriented control	3.7	
Ref. [73]	Power control	Strategy 1	5.6817
		Strategy 2	3.1873
Ref. [74]	DPC strategy with STA controller	1.66	
Ref. [75]	Classical direct torque control	6.70	
	Fuzzy direct torque control	2.40	
Ref. [76]	Direct power control with IP controllers	0.43	
Ref. [77]	Fuzzy sliding mode control	1.15	
Ref. [78]	Direct torque control	7.83	
	Neural direct torque control	3.26	
Ref. [79]	DTC technique using L-filter	10.79	
	DPC strategy using LCL-filter	4.05	
Ref. [80]	Integral sliding mode control	9.71	
	Multi-resonant-based sliding mode controller	3.14	
Ref. [81]	Second-order sliding mode control	3.13	
Ref. [82]	Two-level direct torque control	8.75	
	Three-level direct torque control	1.57	
Ref. [26]	DTC with PI controllers	12	
	DTC strategy with ant colony optimization algorithm	7.19	
Ref. [83]	Virtual flux DPC strategy	4.88	
	DPC	4.19	
Ref. [84]	Predictive polar flux control	0.77	
	Predictive torque control	2.15	
Ref. [85]	Integral sliding mode control	0.88	
Ref. [86]	DTC strategy with genetic algorithm	4.80	
DPC-MSMC technique	First test	0.19	
	Second test	0.40	
	Third test	0.53	

7. Conclusions

In this work, a new method of sliding mode control (called MSMC) was proposed. This proposed method has been applied to the DPC strategy to improve the quality of the powers provided by a DFAG-based MRWT system. The proposed DPC-MSMC technique was achieved using simulation and the obtained results were compared with the classical DPC strategy. The obtained results proved the effectiveness of the proposed modified SMC technique in improving the performance and effectiveness of the DPC method. The results obtained can be summarized in the following points:

1. Improve the effectiveness of the DPC of the DFAG-based MRWT system.

2. The proposed DPC-MSMC technique reduced reactive power, torque, active power, and current ripples compared with the classic DPC method.
3. Decrease the THD value of the electric current.
4. Decrease the steady-state error of the active and reactive powers of the DFAG.
5. The proposed DPC-MSMC technique is more robust compared to the classical DPC strategy.

In the near future, we will verify the performance and control effectiveness of the proposed method on a wind power generation system using grid-connected DFAG to solve problems of ripples for active power and electric current.

Author Contributions: Validation, N.B., P.T. and N.T.; conceptualization, H.B. and Z.B.; software, H.B. and Z.B.; methodology, H.B. and Z.B.; investigation, H.B. and Z.B.; resources, H.B., N.B., P.T. and N.T.; project administration, N.B.; data curation, N.B., P.T. and N.T.; writing—original draft preparation, H.B.; supervision, N.B.; visualization: Z.B. and N.B.; formal analysis: N.B.; funding acquisition: N.B., P.T. and N.T.; writing—review and editing: N.B., P.T., N.T., H.B. and Z.B. All authors have read and agreed to the published version of the manuscript.

Funding: This work was supported in part by the Framework Agreement between University of Pitesti (Romania) and King Mongkut’s University of Technology North Bangkok (Thailand), in part by an International Research Partnership “Electrical Engineering-Thai French Research Center (EE-TFRC)” under the project framework of the Lorraine Université d’Excellence (LUE) in cooperation between Université de Lorraine and King Mongkut’s University of Technology North Bangkok and in part by the National Research Council of Thailand (NRCT) under Senior Research scholar Program under Grant No. N42A640328, and in part by National Science, Research and Innovation Fund (NSRF) under King Mongkut’s University of Technology North Bangkok under Grant No. KMUTNB-FF-65-20.

Institutional Review Board Statement: Not applicable.

Informed Consent Statement: Not applicable.

Data Availability Statement: Not applicable.

Conflicts of Interest: The authors declare no conflict of interest.

Abbreviations

SMC	Sliding mode control
DTC	Direct torque control
SOSMC	Second-order sliding mode control
FOC	Field-oriented control
DPC	Direct power control
MSMC	Modified sliding mode control
PI	Proportional-integral
THD	Total harmonic distortion
BC	Backstepping control
DFAG	Doubly fed asynchronous generator
MRWT	Multi-rotor wind turbine
PWM	Pulse width modulation
MPPT	Maximum point power tracking technique
RSC	Rotor side converter
SSC	Stator side converter
GSC	Generator side converter
GA	Genetic algorithm
ACO	Ant colony optimization

References

1. Fontecha, R.; Kemper, F.; Feldmann, M.; Witter, S.; Schelenz, R. Along-Wind Aerodynamic Damping of Wind Turbine Towers: Determination by Wind Tunnel Tests and Impact on Tower Lifetime. *Energies* **2022**, *15*, 1984. [CrossRef]
2. Lu, L.; Saborío-Romano, O.; Cutululis, N.A. Frequency Control in Power Systems with Large Share of Wind Energy. *Energies* **2022**, *15*, 1922. [CrossRef]
3. Cardoni, M.; Pau, D.P.; Falaschetti, L.; Turchetti, C.; Lattuada, M. Online Learning of Oil Leak Anomalies in Wind Turbines with Block-Based Binary Reservoir. *Electronics* **2021**, *10*, 2836. [CrossRef]
4. Gutiérrez, F.E.R.; Castillo, O.C.; Rivas, J.J.R.; González, R.O.; Sánchez, E.P.; González Morales, L.G. Harmonics Reduction and Reactive Power Injection in Wind Generation Systems. *Electronics* **2021**, *10*, 1964. [CrossRef]
5. Volosencu, C. A Comparative Analysis of Some Methods for Wind Turbine Maximum Power Point Tracking. *Mathematics* **2021**, *9*, 2399. [CrossRef]
6. Chen, Z.; Yin, M.; Zou, Y.; Meng, K.; Dong, Z.Y. Maximum Wind Energy Extraction for Variable Speed Wind Turbines with Slow Dynamic Behavior. *IEEE Trans. Power Syst.* **2017**, *32*, 3321–3322. [CrossRef]
7. Jafarnejadsani, H.; Pieper, J.; Ehlers, J. Adaptive Control of a Variable-Speed Variable-Pitch Wind Turbine Using Radial-Basis Function Neural Network. *IEEE Trans. Control Syst.* **2013**, *21*, 2264–2272. [CrossRef]
8. Zou, Z.-C.; Xiao, X.-Y.; Liu, Y.-F.; Zhang, Y.; Wang, Y.-H. Integrated Protection of DFIG-Based Wind Turbine with a Resistive-Type SFCL Under Symmetrical and Asymmetrical Faults. *IEEE Trans. Appl. Supercond.* **2016**, *26*, 5603005. [CrossRef]
9. Verma, P.; Seethalekshmi, K.; Dwivedi, B. A Cooperative Approach of Frequency Regulation through Virtual Inertia Control and Enhancement of Low Voltage Ride-Through in DFIG-Based Wind Farm. *J. Mod. Power Syst. Clean Energy* **2021**. [CrossRef]
10. Wang, M.; Chen, Y.; Dong, X.; Hu, S.; Liu, B.; Samson, S.Y.; Liu, X. Impedance Modeling and Stability Analysis of DFIG Wind Farm with LCC-HVDC Transmission. in *IEEE Journal on Emerging and Selected Topics in Circuits and Systems*. *IEEE J. Emerg. Sel. Top. Circuits Syst.* **2022**, *12*, 7–19. [CrossRef]
11. Nnem, L.M.; Lonla, B.M.; Sonfack, G.B.; Mbih, J. Review of a Multipurpose Duty-Cycle Modulation Technology in Electrical and Electronics Engineering. *J. Electr. Eng. Electron. Control Comput. Sci.* **2018**, *4*, 9–18. Available online: <https://jeeccs.net/index.php/journal/article/view/101> (accessed on 21 April 2022).
12. Xie, Z.; Feng, Y.; Ma, M.; Zhang, X. An Improved Virtual Inertia Control Strategy of DFIG-Based Wind Turbines for Grid Frequency Support. *IEEE J. Emerg. Sel. Top. Power Electron.* **2021**, *9*, 5465–5477. [CrossRef]
13. Ahmed, T.; Nishida, K.; Nakaoka, M. A novel stand-alone induction generator system for AC and DC power applications. *IEEE Trans. Ind. Appl.* **2007**, *43*, 1465–1474. [CrossRef]
14. Mondal, S.; Kastha, D. Input Reactive Power Controller with a Novel Active Damping Strategy for a Matrix Converter Fed Direct Torque Controlled DFIG for Wind Power Generation. *IEEE J. Emerg. Sel. Top. Power Electron.* **2020**, *8*, 3700–3711. [CrossRef]
15. Xiong, L.; Li, P.; Li, H.; Wang, J. Sliding Mode Control of DFIG Wind Turbines with a Fast Exponential Reaching Law. *Energies* **2017**, *10*, 1788. [CrossRef]
16. Morawiec, M.; Blecharz, K.; Lewicki, A. Sensorless Rotor Position Estimation of Doubly Fed Induction Generator Based on Backstepping Technique. *IEEE Trans. Ind. Electron.* **2020**, *67*, 5889–5899. [CrossRef]
17. Nair, R.; Narayanan, G. Stator Flux Based Model Reference Adaptive Observers for Sensorless Vector Control and Direct Voltage Control of Doubly-Fed Induction Generator. *IEEE Trans. Ind. Appl.* **2020**, *56*, 3776–3789. [CrossRef]
18. Benbouhenni, H. Synergetic control theory scheme for asynchronous generator based dual-rotor wind power. *J. Electr. Eng. Electron. Control Comput. Sci.* **2021**, *7*, 19–28. Available online: <https://jeeccs.net/index.php/journal/article/view/215> (accessed on 5 May 2022).
19. Mohammadi, J.; Vaez-Zadeh, S.; Afsharnia, S.; Daryabeigi, E. A Combined Vector and Direct Power Control for DFIG-Based Wind Turbines. *IEEE Trans. Sustain. Energy* **2014**, *5*, 767–775. [CrossRef]
20. Hu, B.; Nian, H.; Yang, J.; Li, M.; Xu, Y. High-Frequency Resonance Analysis and Reshaping Control Strategy of DFIG System Based on DPC. *IEEE Trans. Power Electron.* **2021**, *36*, 7810–7819. [CrossRef]
21. Prasad, R.M.; Mulla, M.A. A Novel Position-Sensorless Algorithm for Field-Oriented Control of DFIG With Reduced Current Sensors. *IEEE Trans. Sustain. Energy* **2019**, *10*, 1098–1108. [CrossRef]
22. Zhibin, Z.; Hao, C.; Wei, X.; Xiyang, C.; Jingang, H.; Nadia, A.; Tianhao, T.; Mohamed, B. Fractional-Order PI Control of DFIG-Based Tidal Stream Turbine. *J. Mar. Sci. Eng.* **2020**, *8*, 309. [CrossRef]
23. Benbouhenni, H.; Boudjema, Z.; Belaidi, A. Power Control of DFIG in WECS Using DPC and NDPC-NPWM Methods. *Math. Model. Eng. Probl.* **2020**, *7*, 223–236. [CrossRef]
24. Sahri, Y.; Tamalouzt, S.; Lalouni Belaid, S.; Bacha, S.; Ullah, N.; Ahamdi, A.A.A.; Alzaed, A.N. Advanced Fuzzy 12 DTC Control of Doubly Fed Induction Generator for Optimal Power Extraction in Wind Turbine System under Random Wind Conditions. *Sustainability* **2021**, *13*, 11593. [CrossRef]
25. Benbouhenni, H. Application of DPC and DPC-GA to the dual-rotor wind turbine system with DFIG. *Int. J. Robot. Autom.* **2021**, *10*, 224–234. [CrossRef]
26. Mahfoud, S.; Derouch, A.; Iqbal, A.; El Ouanjli, N. Ant-Colony optimization-direct torque control for a doubly fed induction motor: An experimental validation. *Energy Rep.* **2022**, *8*, 81–98. [CrossRef]
27. Xiong, P.; Sun, D. Backstepping-Based DPC Strategy of a Wind Turbine-Driven DFIG Under Normal and Harmonic Grid Voltage. *IEEE Trans. Power Electron.* **2016**, *31*, 4216–4225. [CrossRef]

28. Mazen Alhato, M.; Bouallègue, S.; Rezk, H. Modeling and Performance Improvement of Direct Power Control of Doubly-Fed Induction Generator Based Wind Turbine through Second-Order Sliding Mode Control Approach. *Mathematics* **2020**, *8*, 2012. [[CrossRef](#)]
29. Han, Y.; Ma, R. Adaptive-Gain Second-Order Sliding Mode Direct Power Control for Wind-Turbine-Driven DFIG under Balanced and Unbalanced Grid Voltage. *Energies* **2019**, *12*, 3886. [[CrossRef](#)]
30. Utkin, V. Survey paper variable structure systems with sliding modes. *IEEE Trans. Autom. Control* **1977**, *22*, 212–222. [[CrossRef](#)]
31. Mi, Y.; Song, Y.; Fu, Y.; Wang, C. The Adaptive Sliding Mode Reactive Power Control Strategy for Wind–Diesel Power System Based on Sliding Mode Observer. *IEEE Trans. Sustain. Energy* **2020**, *11*, 2241–2251. [[CrossRef](#)]
32. De Battista, H.; Mantz, R.J.; Christiansen, C.F. Dynamical sliding mode power control of wind driven induction generators. *IEEE Trans. Energy Conver.* **2000**, *15*, 451–457. [[CrossRef](#)]
33. Beltran, B.; Ahmed-Ali, T.; El Hachemi, B.M. Sliding Mode Power Control of Variable-Speed Wind Energy Conversion Systems. *IEEE Trans. Energy Conver.* **2008**, *23*, 551–558. [[CrossRef](#)]
34. Merabet, A.; Ahmed, K.T.; Ibrahim, H.; Beguenane, R. Implementation of Sliding Mode Control System for Generator and Grid Sides Control of Wind Energy Conversion System. *IEEE Trans. Sustain Energy* **2016**, *7*, 1327–1335. [[CrossRef](#)]
35. Utkin, V.I. *Sliding Modes in Control and Optimization*; Springer: Berlin/Heidelberg, Germany, 1992.
36. Gao, Q.; Liu, L.; Feng, G.; Wang, Y. Universal Fuzzy Integral Sliding-Mode Controllers for Stochastic Nonlinear Systems. *IEEE Trans. Cybern.* **2014**, *44*, 2658–2669. [[CrossRef](#)]
37. Saghafinia, A.; Ping, H.W.; Uddin, M.N.; Gaeid, K.S. Adaptive Fuzzy Sliding-Mode Control into Chattering-Free IM Drive. *IEEE Trans. Ind. Appl.* **2015**, *51*, 692–701. [[CrossRef](#)]
38. Parma, G.G.; Menezes, B.R.; Braga, A.P.; Costa, M.A. Sliding mode neural network control of an induction motor drive. *Int. J. Adapt. Control* **2003**, *17*, 501–508. [[CrossRef](#)]
39. Djilali, L.; Sanchez, E.N.; Belkheiri, M. Real-time neural sliding mode field oriented control for a DFIG-based wind turbine under balanced and unbalanced grid conditions. *IET Renew Power Gener.* **2019**, *13*, 618–632. [[CrossRef](#)]
40. Ding, S.; Li, S.; Zheng, W.X. New approach to second-order sliding mode control design. *IET Control Theory Appl.* **2013**, *7*, 2188–2196. [[CrossRef](#)]
41. Junejo, A.K.; Xu, W.; Mu, C.; Ismail, M.M.; Liu, Y. Adaptive Speed Control of PMSM Drive System Based a New Sliding-Mode Reaching Law. *IEEE Trans. Power Electr.* **2020**, *35*, 12110–12121. [[CrossRef](#)]
42. Chen, X.; Li, Y.; Ma, H.; Tang, H.; Xie, Y. A Novel Variable Exponential Discrete Time Sliding Mode Reaching Law. *IEEE Trans. Circuits Syst. Express Briefs* **2021**, *68*, 2518–2522. [[CrossRef](#)]
43. Huang, S.; Xiong, L.; Wang, J.; Li, P.; Wang, Z.; Ma, M. Fixed-Time Fractional-Order Sliding Mode Controller for Multimachine Power Systems. *IEEE Trans. Power Syst.* **2021**, *36*, 2866–2876. [[CrossRef](#)]
44. Li, P.; Wang, J.; Xiong, L.; Huang, S.; Wang, Z.; Ma, M. SSCI mitigation of grid-connected DFIG wind turbines with fractional-order sliding mode controller. *Wind Energy* **2020**, *23*, 1564–1577. [[CrossRef](#)]
45. Talebi, J.; Ganjefar, S. Fractional order sliding mode controller design for large scale variable speed wind turbine for power optimization. *Environ. Prog. Sustain.* **2018**, *37*, 2124–2131. [[CrossRef](#)]
46. Rui, X.; Yin, W.; Dong, Y.; Lin, L.; Wu, X. Fractional-order sliding mode control for hybrid drive wind power generation system with disturbances in the grid. *Wind Energy* **2019**, *22*, 49–64. [[CrossRef](#)]
47. Xiong, X.; Kamal, S.; Jin, S. Adaptive gains to super-twisting technique for sliding mode design. *Asian J. Control* **2019**, *23*, 362–373. [[CrossRef](#)]
48. Chen, C.; Yu, H. Backstepping sliding mode control of induction motor based on disturbance observer. *IET Electr. Power Appl.* **2020**, *14*, 2537–2546. [[CrossRef](#)]
49. Hu, W.; Ding, F.; Zhang, J.; Zhang, B.; Zhang, N.; Qin, A. Robust adaptive backstepping sliding mode control for motion mode decoupling of two-axle vehicles with active kinetic dynamic suspension systems. *Int. J. Robust Nonlin.* **2020**, *30*, 3110–3133. [[CrossRef](#)]
50. Li, F.; Du, C.; Yang, C.; Gui, W. Passivity-Based Asynchronous Sliding Mode Control for Delayed Singular Markovian Jump Systems. *IEEE Trans. Autom. Control* **2018**, *63*, 2715–2721. [[CrossRef](#)]
51. Fujimoto, K.; Sakata, N.; Maruta, I.; Ferguson, J. A Passivity Based Sliding Mode Controller for Simple Port-Hamiltonian Systems. *IEEE Control Syst. Lett.* **2021**, *5*, 839–844. [[CrossRef](#)]
52. Zhang, X.; Huang, W.; Wang, Q.G. Robust H_∞ Adaptive Sliding Mode Fault Tolerant Control for T-S Fuzzy Fractional Order Systems with Mismatched Disturbances. *IEEE Trans. Circuits Syst.* **2021**, *68*, 1297–1307. [[CrossRef](#)]
53. He, L.; Wang, F.; Ke, D. FPGA-Based Sliding-Mode Predictive Control for PMSM Speed Regulation System Using an Adaptive Ultralocal Model. *IEEE Trans. Power Electr.* **2021**, *36*, 5784–5793. [[CrossRef](#)]
54. Huang, C.; Naghdy, F.; Du, H. Fault Tolerant Sliding Mode Predictive Control for Uncertain Steer-by-Wire System. *IEEE Trans. Cybern.* **2019**, *49*, 261–272. [[CrossRef](#)] [[PubMed](#)]
55. Benbouhenni, H.; Bizon, N. Advanced direct vector control method for optimizing the operation of a double-powered induction generator-based dual-rotor wind turbine system. *Mathematics* **2021**, *9*, 2403. [[CrossRef](#)]
56. Benbouhenni, H.; Bizon, N. A Synergetic Sliding Mode Controller Applied to Direct Field-Oriented Control of Induction Generator-Based Variable Speed Dual-Rotor Wind Turbines. *Energies* **2021**, *14*, 4437. [[CrossRef](#)]

57. Benbouhenni, H.; Bizon, N. Terminal Synergetic Control for Direct Active and Reactive Powers in Asynchronous Generator-Based Dual-Rotor Wind Power Systems. *Electronics* **2021**, *10*, 1880. [CrossRef]
58. Shahzad, U. Application of Machine Learning for Optimal Wind Farm Location. *J. Electr. Eng. Electron. Control Comput. Sci.* **2022**, *8*, 1–8. Available online: <https://jeeeccs.net/index.php/journal/article/view/276> (accessed on 21 April 2022).
59. Velpula, S.; Thirumalaivasan, R.; Janaki, M. Stability Analysis on Torsional Interactions of Turbine-Generator Connected With DFIG-WECS Using Admittance Model. *IEEE Trans. Power Syst.* **2020**, *35*, 4745–4755. [CrossRef]
60. Giaourakis, D.G.; Safacas, A.N. Effect of Short-Circuit Faults in the Back-to-Back Power Electronic Converter and Rotor Terminals on the Operational Behavior of the Doubly-Fed Induction Generator Wind Energy Conversion System. *Machines* **2015**, *3*, 2–26. [CrossRef]
61. Pan, L.; Zhu, Z.; Xiong, Y.; Shao, J. Integral Sliding Mode Control for Maximum Power Point Tracking in DFIG Based Floating Offshore Wind Turbine and Power to Gas. *Processes* **2021**, *9*, 1016. [CrossRef]
62. Sami, I.; Ullah, S.; Ali, Z.; Ullah, N.; Ro, J.-S. A Super Twisting Fractional Order Terminal Sliding Mode Control for DFIG-Based Wind Energy Conversion System. *Energies* **2020**, *13*, 2158. [CrossRef]
63. Mohamed Ahmed, S.A.; Montaser Abd El Sattar, M.A. Dynamic Performance and Effectiveness of Voltage Disturbances on the Improvement of Power Quality for Grid-Connected DFIG System Based Wind Farm. *J. Electr. Eng. Electron. Control Comput. Sci.* **2020**, *5*, 25–30. Available online: <https://jeeeccs.net/index.php/journal/article/view/126> (accessed on 21 April 2022).
64. Susperregui, A.; Herrero, J.M.; Martinez, M.I.; Tapia-Otaegui, G.; Blasco, X. Multi-Objective Optimisation-Based Tuning of Two Second-Order Sliding-Mode Controller Variants for DFIGs Connected to Non-Ideal Grid Voltage. *Energies* **2019**, *12*, 3782. [CrossRef]
65. Kong, H.; He, J.; Liu, Y.; Cheng, P.; Ma, J. Improved Direct Power Control of Doubly Fed Induction Generator Without Phase-Locked Loop. In Proceedings of the IEEE Sustainable Power and Energy Conference (iSPEC), Chengdu, China, 23–25 November 2020; pp. 199–204. [CrossRef]
66. Zhang, Y.; Jiao, J.; Xu, D. Direct Power Control of Doubly Fed Induction Generator Using Extended Power Theory Under Unbalanced Network. *IEEE Trans. Power Electron.* **2019**, *34*, 12024–12037. [CrossRef]
67. Zarei, M.E.; Nicolás, C.V.; Arribas, J.R.; Ramírez, D. Four-Switch Three-Phase Operation of Grid-Side Converter of Doubly Fed Induction Generator with Three Vectors Predictive Direct Power Control Strategy. *IEEE Trans. Ind. Electron.* **2019**, *66*, 7741–7752. [CrossRef]
68. Santos-Martin, D.; Rodriguez-Amenedo, J.L.; Arnalte, S. Direct Power Control Applied to Doubly Fed Induction Generator Under Unbalanced Grid Voltage Conditions. *IEEE Trans. Power Electron.* **2008**, *23*, 2328–2336. [CrossRef]
69. Benbouhenni, H.; Bizon, N. Third-Order Sliding Mode Applied to the Direct Field-Oriented Control of the Asynchronous Generator for Variable-Speed Contra-Rotating Wind Turbine Generation Systems. *Energies* **2021**, *14*, 5877. [CrossRef]
70. Benbouhenni, H.; Bizon, N. Improved Rotor Flux and Torque Control Based on the Third-Order Sliding Mode Scheme Applied to the Asynchronous Generator for the Single-Rotor Wind Turbine. *Mathematics* **2021**, *9*, 2297. [CrossRef]
71. Kamarzarrin, M.; Refan, M.H.; Amiri, P.; Dameshghi, A. Fault Diagnosis of Wind Turbine Double-Fed Induction Generator Based on Multi-Level Fusion and Measurement of Back-to-Back Converter Current Signal. *Iran. J. Electr. Electron. Eng.* **2022**, *18*, 2074.
72. Amrane, F.; Chaiba, A.; Babas, B.E.; Mekhilef, S. Design and implementation of high performance field oriented control for grid-connected doubly fed induction generator via hysteresis rotor current controller. *Rev. Roum. Sci. Tech. Électrotech. Énerg.* **2016**, *61*, 319–324.
73. Moreira, A.B.; Barros, T.A.D.S.; Teixeira, V.S.D.C.; Souza, R.R.D.; Paula, M.V.D.; Filho, E.R. Control of Powers for Wind Power Generation and Grid Current Harmonics Filtering from Doubly Fed Induction Generator: Comparison of Two Strategies. *IEEE Access* **2019**, *7*, 32703–32713. [CrossRef]
74. Yaichi, I.; Semmah, A.; Wira, P.; Djeriri, Y. Super-twisting sliding mode control of a doubly-fed induction generator based on the SVM strategy. *Period. Polytech. Electr. Eng. Comput. Sci.* **2019**, *63*, 178–190. [CrossRef]
75. Ayrira, W.; Ourahoua, M.; El Hassounia, B.; Haddib, A. Direct torque control improvement of a variable speed DFIG based on a fuzzy inference system. *Math. Comput. Simul.* **2020**, *167*, 308–324. [CrossRef]
76. Fayssal, A.; Bruno, F.; Azeddine, C. Experimental investigation of efficient and simple wind-turbine based on DFIG-direct power control using LCL-filter for stand-alone mode. *ISA Trans.* **2021**, 1–34, *in press*. [CrossRef]
77. Boudjema, Z.; Meroufel, A.; Djerriri, Y.; Bounadja, E. Fuzzy sliding mode control of a doubly fed induction generator for energy conversion. *Carpathian J. Electron. Comput. Eng.* **2013**, *6*, 7–14.
78. Said, M.; Derouich, A.; El Ouanjli, N.; El Mahfoud, M. Enhancement of the Direct Torque Control by using Artificial Neuron Network for a Doubly Fed Induction Motor. *Intell. Syst. Appl.* **2022**, *13*, 200060. [CrossRef]
79. Alhato, M.M.; Bouallègue, S. Direct Power Control Optimization for Doubly Fed Induction Generator Based Wind Turbine Systems. *Math. Comput. Appl.* **2019**, *24*, 77. [CrossRef]
80. Quan, Y.; Hang, L.; He, Y.; Zhang, Y. Multi-Resonant-Based Sliding Mode Control of DFIG-Based Wind System under Unbalanced and Harmonic Network Conditions. *Appl. Sci.* **2019**, *9*, 1124. [CrossRef]
81. Yahdou, A.; Hemici, B.; Boudjema, Z. Second order sliding mode control of a dual-rotor wind turbine system by employing a matrix converter. *J. Electr. Eng.* **2016**, *16*, 11.
82. Najib, E.; Aziz, D.; Abdelaziz, E.; Mohammed, T.; Youness, E.; Khalid, M.; Badre, B. Direct torque control of doubly fed induction motor using three-level NPC inverter. *Prot. Control Mod. Power Syst.* **2019**, *4*, 1–9. [CrossRef]

83. Yusoff, N.A.; Razali, A.M.; Karim, K.A.; Sutikno, T.; Jidin, A. A concept of virtual-flux direct power control of three-phase AC-DC converter. *Int. J. Power Electron. Drive Syst.* **2017**, *8*, 1776–1784. [[CrossRef](#)]
84. Mahmoud, A.M.; Echeikh, H.; Atif, I. Enhanced control technique for a sensor-less wind driven doubly fed induction generator for energy conversion purpose. *Energy Rep.* **2021**, *7*, 5815–5833. [[CrossRef](#)]
85. Hamid, C.; Aziz, D.; Seif Eddine, C.; Othmane, Z.; Mohammed, T.; Hasnae, E. Integral sliding mode control for DFIG based WECS with MPPT based on artificial neural network under a real wind profile. *Energy Rep.* **2021**, *7*, 4809–4824. [[CrossRef](#)]
86. Mahfoud, S.; Derouich, A.; El Ouanjli, N.; El Mahfoud, M.; Taoussi, M. A New Strategy-Based PID Controller Optimized by Genetic Algorithm for DTC of the Doubly Fed Induction Motor. *Systems* **2021**, *9*, 37. [[CrossRef](#)]